Report IFJ No 1973/AP

Development of the IFJ Single Ion Hit facility for cells irradiation.

O. Veselov, W. Polak, R. Ugenskiene, R. Hajduk, K. Lebed,
J. Lekki, T. Horwacik, E.M. Dutkiewicz, S. Maranda,
T. Pieprzyca, C. Sarnecki, Z. Stachura, Z. Szklarz, J. Styczeń

Abstract

In recent years a single ion hit facility (SIHF) has been constructed at the IFJ ion microprobe. The setup is used for the precise irradiations of living cells by a controlled number of ions. The facility allows investigations in various aspects of biomedical research, such as adaptive response, bystander effect, inverse dose-rate effect, low-dose hypersensitivity, etc.

Those investigations have two very important requirements: (i) cells must be examined in their natural state and environment, i.e. without previously being killed, and preferentially, neither fixed nor stained, and (ii) a possibility of automatic irradiation of large number of cells with a computer recognition of their positions must be provided.

This work presents some of the crucial features of the off-line and on-line optical systems, including self-developed software responsible for the automatic cell recognition. We also show several tests carried out to determine the efficiency of the whole setup and some segments. In conclusion, the results of our first irradiation measurements performed with living cells are demonstrated.

This study was supported by the project CELLION of the EU 6th Framework Programme, No MRTN-CT-2003-503923.

Introduction

Recent years have brought a number of scientific papers related to microprobe facilities application studies of radiation–induced cellular response [1-13]. The obtained results have shown a need for those studies to be continued. The main interest has been broadened by the anomalous effects observed during the low-dose irradiation such as adaptive response, bystander effect, inverse dose-rate effect, low-dose hypersensitivity etc.

Studies of this kind require developing of microprobe–based single ion hit facility [31, 32] used for studying abovementioned effects via the irradiation of selected cells (or cell compartments) with a well–defined dose and with accurate knowledge of the ion track. It should be noted that, occasionally, for such type of measurements it is necessary to irradiate several thousands of cells during one experiment. In the experiment, living cells must be taken out from their native environment (incubator conditions) and positioned in the microprobe facility. The time for carrying out the experiment should be therefore rather short, in spite of the fact that often a large number of cells must be irradiated. For this purpose, an important requirement is to automate the processes of the target cell identification.

The Single Ion Hit Facility (SIHF) at IFJ PAN, Cracow, is utilizing a Van de Graaff accelerator–based microprobe [14, 15]. The schematic view of the facility is presented in Fig. 1.

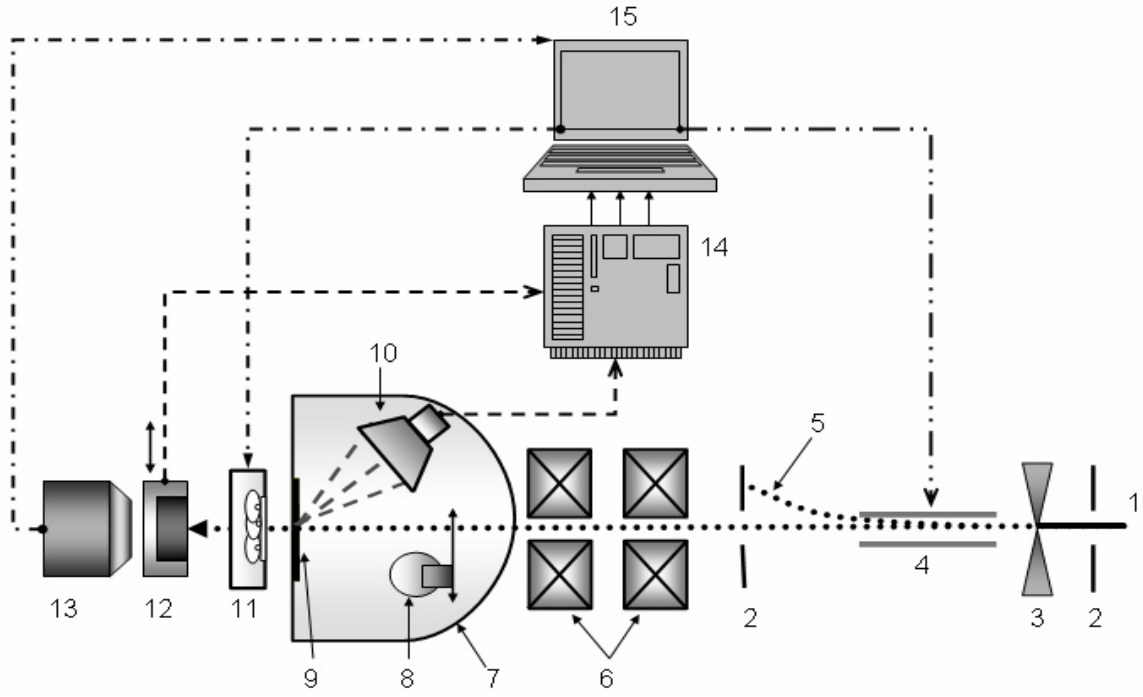

Fig.1 *Schematic view of the Single Ion Hit Facility in Cracow.*

The proton beam (1), passing through a 90° analysing magnet and pre-focused with 3 doublets of quadrupoles, enters the SIHF. The beam size and position is set by two diaphragms (2). Subsequently, the precise diaphragms (3) reduce the beam current to a fraction of fA that corresponds to about 1000 protons/s. After that, two electrostatic deflecting plates (4) (Technisches Büro S. Fisher) mounted after the slits allow rapid beam blanking (5). Then, the beam is focused with two doublets of quadrupoles (MARC, Melbourne, Australia) (6). The main measurement stage consists of a chamber (7) (including: high brightness LED diode (8), Si_3N_4 exit window (9) and a channeltron (10)), a 3D moving stage[11] equipped with a Petri-dish as a cell container, a particle silicon

surface barrier detector (ORTEC) positioned on a moving arm (12), and microscope with CCD camera (13). The central unit of the system is a computer (15) which directly controls positioning and blanking processes and collects information from the microscope and the detectors using an electronic data acquisition system (14).

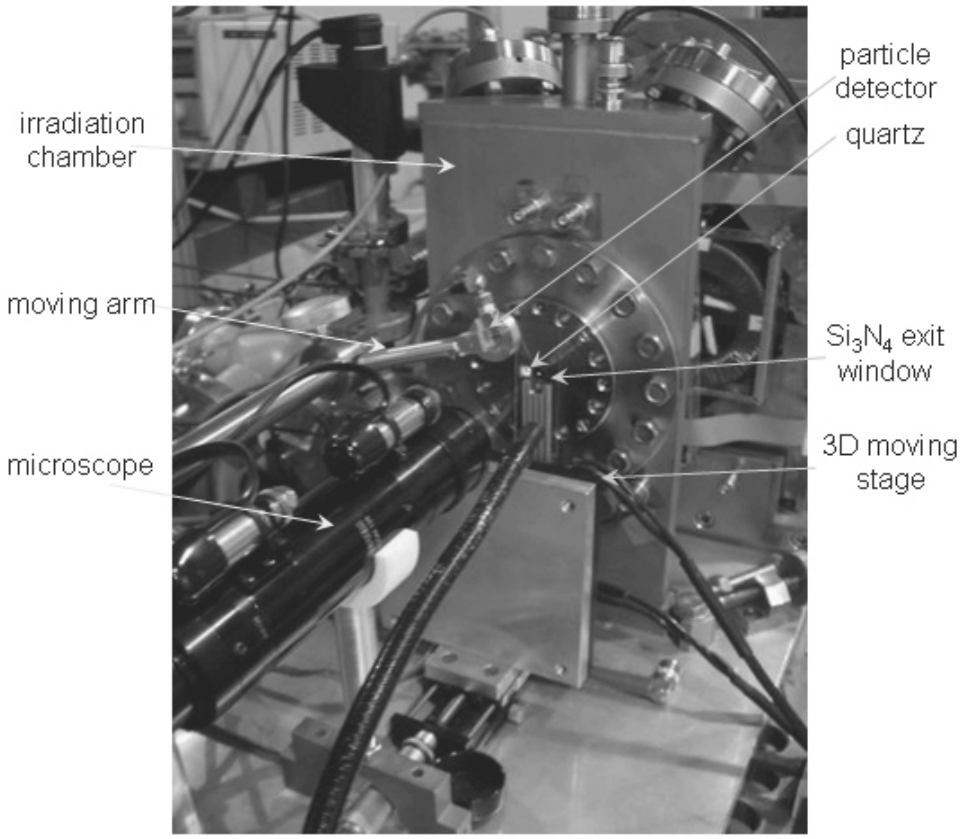

Fig. 2 *Front view of the SIH facility showing its main modules: the irradiation chamber, the on-line microscope, the particle detector and the precise 3D moving stage.*

The facility is equipped also in two optical systems for cell visualisation and examination: the off–line setup (i.e. located in the sample preparation room) and the on–line one (at the experimental chamber). During experiments both systems are used in basically different applications.

Off-line optical system

It the SIH studies, observation and evaluation of cell samples before and after the experiment is very important. Therefore, we have installed a high quality optical system, which is based on Olympus BX51 microscope with brightfield illumination and 4x, 10x, 20x, 50x objectives and an automatic, computer controlled moving stage. Moreover, the system includes tools both for fluorescent microscopy and Quantitative Phase microscopy (QPm) [18, 20]. The fluorescent microscopy is widely used for the visualisation of the transparent samples via their staining. Unfortunately, staining can affect living cells. On the other hand, this technique can be useful as a control for other microscopy methods.

The Quantitative Phase microscopy is the newest breakthrough in the visualisation of the transparent samples. QPm is an image-capturing and analysis tool that is available from the IATIA Company (Australia). The method is based on a patented digital QPI algorithm (Quantitative Phase Imaging) and delivers well separated quantitative phase and amplitude (intensity) information. It should be stressed that no other phase

visualization technique gives phase information only – the phase image contains always some intensity information, too.

The QPI algorithm is based on the paraxial approximation of the intensity propagation distribution as described by the Transport of Intensity Equation [16]

$$k\partial_z I(\vec{r}) = \nabla_\perp \cdot \left[I(\vec{r}) \nabla_\perp \varphi(\vec{r}) \right],$$

where the light at wavelength λ travels along the z direction.

In the above equation $k = \frac{2\pi}{\lambda}$, $\vec{r} = (x, y)$, $I(\vec{r})$ is the irradiance, $\varphi(\vec{r})$ is the phase and $\nabla_\perp = \left(\frac{\partial}{\partial x}, \frac{\partial}{\partial y} \right)$.

The solution for phase in the Transport of Intensity Equation can be presented in the following form

$$\varphi = -\bar{k} \nabla_\perp^{-2} \left\{ \nabla_\perp \cdot \left[\frac{1}{\bar{I}} \nabla_\perp \nabla_\perp^{-2} \partial_z \bar{I} \right] \right\}.$$

The ability of the QPI algorithm regains phase information from only two ordinary brightfield images which are taken on slightly different focal planes (Fig.3). In addition, a third image is taken at the focus plane generally for normalisation. The phase data is rendered as a grey scale image (the phase map), and represents the phase or optical density across a sample that is entirely free of intensity based data.

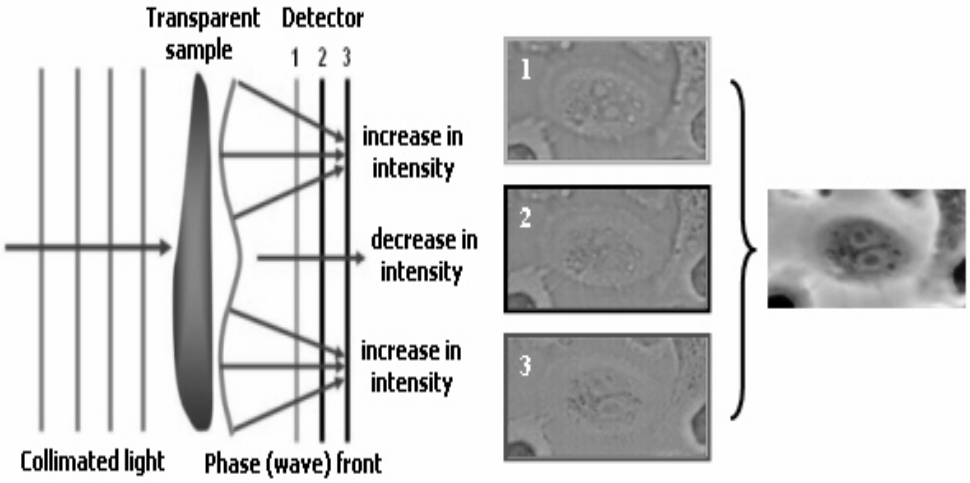

Fig. 3 *Principle of the Quantitative Phase microscopy*

QPm has a number of key advantages. For current application particularly useful are:

– independent calculation of phase and intensity
– determination of quantitative, absolute phase
– fast, stable, non-iterative algorithm
– possibility of using a non-uniform and partially coherent illumination.

The phase images can be used as they are, or can be used to simulate 'Standard Phase Contrast' (e.g. Zernike Phase Contrast), 'Differential Interference Contrast' (DIC), 'Hoffman Modulation Contrast' (HMC).

When using QPm, the application of staining to enhance the intensity contrast of an

image is unnecessary. Stains are taken up in varying degrees by the refractive components of the sample to give an image with a defined relationship between intensity and refraction. Fig.4 compares a 'brightfield image' of a cell culture and a 'QPm' result.

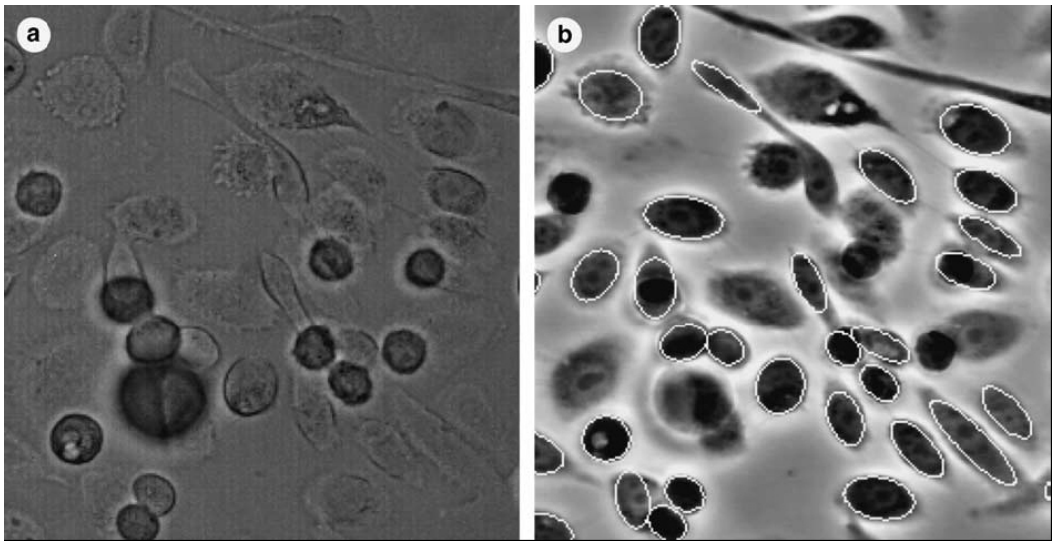

Fig. 4 *Images taken with 20X magnification of live unstained human prostatic adenocarcinoma cells plated on the bottom of Petri dish; (a) – the brightfield image, (b) – QPm pure phase image. Objects recognized by the program as cells are marked by white ellipses (b). The displayed area is 100 x 100 µm^2, what was cut from a large image of 1.31 megapixel source data (1280x1024 pixels, 480 x 385 µm^2). The processing of this large image took about 5 seconds using Athlon XP 2800+ PC.*

Due to the transparency of the sample, the intensity information of the background is similar to the cytoplasm area in the brightfield image and the cells are nearly invisible (Fig.4.a). Whereas the QPm (Fig.4.b) displays larger contrast by calculating the phase shift through each point in the image. The cells contain a medium of higher refractive index compared to the background and the light travels slower through the cell than through its external environment. This 'phase shift' or 'retarding' of the light is a principle by which QPm can differentiate various objects. In the phase image (Fig.4.b) one can even see some structural details of the cell, e.g. nuclei. To demonstrate the difficulties in cell recognition, the image in Fig.4 was chosen from the area where many debris particles are visible, the cells vary considerably in size, cells of unusual shapes can be observed and groups of overlapping cells are present.

The off-line system is supported by the commercial Image-Pro Plus 5.0 analysis package (Media Cybernetics [17]) that contains modules of objects recognition and counting. The example of the cells recognition (white circular markers) is also presented in Fig.4b.

The on-line optical system

The recent improvement of the irradiation setup via the introduction of the high brightness LED diode inside the experimental chamber allows also the on–line observation of the unstained cells (see Fig.5) in the transmitted light using a standard microscope objective. By moving the LED off-axis of the microscope, a partially dark-field image was obtained. This allows for convenient observation of cells just prior to ion irradiation, see Figure 5.

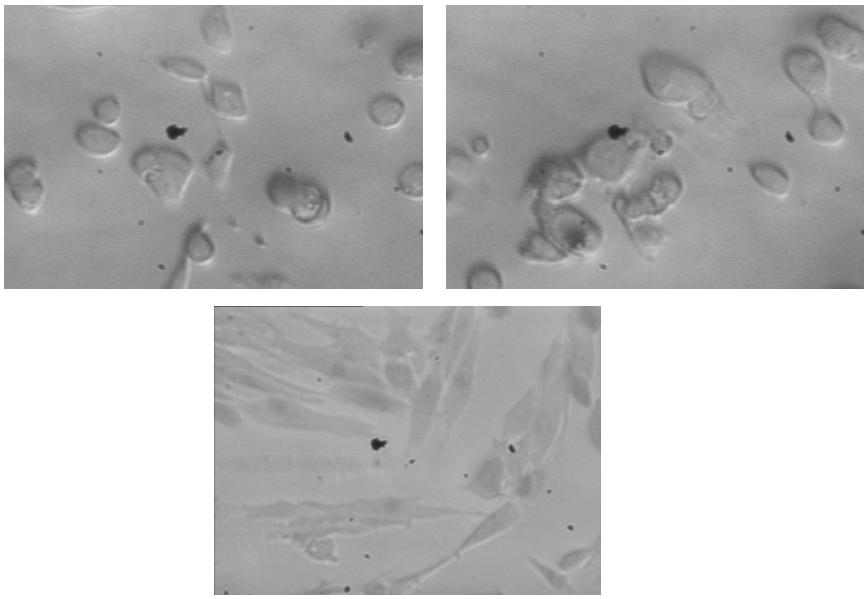

Fig. 5 *On-line images of living cells captured during the experiment at the irradiation setup: top – well differentiated gastric adenocarcinoma cells, bottom – human fibroblasts. The field of view is about 300x200 μm^2.*

The images presented in the Fig.5 are obtained using the on-line optical system with the B/W CCTV Camera SG32M-1CE AI/DC [19] characterized by a high sensitivity of 0.01 lx/F 1.4.
The acquired images are the input data for the further image processing.

Image processing for cell recognition.

The main aim of image processing is to find cell coordinates in a microscopic image. Subsequently, these coordinates are used in the microprobe control program responsible for the cell irradiation process.

Generally, image processing has at its disposal a great number of transformation procedures (filters, logical operations, morphological transformations etc.). Nevertheless, there is no one universal way to get the required result. Therefore, the image analysis is usually performed as a sequence of consecutive procedures.

First, an attempt has been done to find the proper procedure sequence [18] with a help of the Image-Pro 5 program. However, the application of this package has encountered several problems, such as difficulty to integrate the Image-Pro into the program controlling the irradiation process or the absence of specialized methods (e.g. Hough transform) in the image processing functions library. Therefore, it has been decided to rather develop a tailored code for cells recognition and to integrate it into the microprobe

control software.

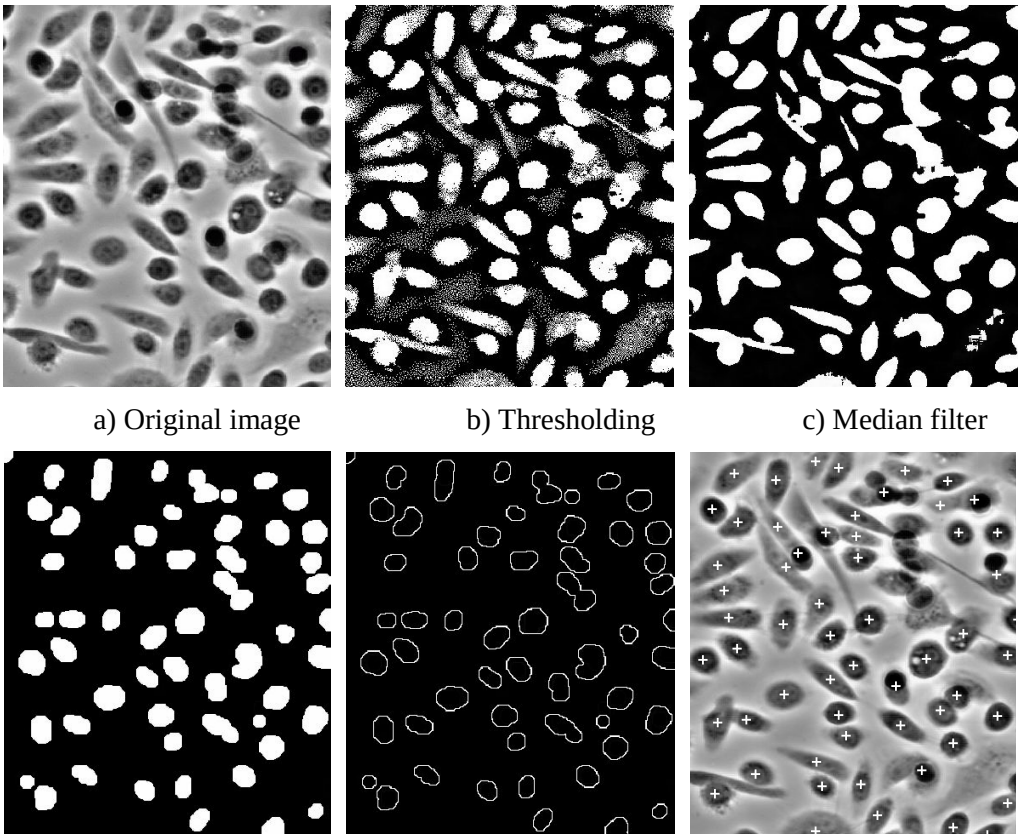

a) Original image b) Thresholding c) Median filter

d) Opening transformation e) Sobel operators f) Hough transform

Fig.6. *The example of image processing. For demonstration purposes, only a small portion of the whole image is shown in such a way that an output image of each step is an input for the next step.*

The presented software is based on several procedures (see Fig.6) interacting in such a flexible way that it allows to adjust and modify the applied algorithm from the simple case (for fast preliminary investigation) to the compound sequences of image transformations (for precise cell recognition).

Although the methods used are well-known and commonly applied [21, 22], it is worth to notice several details, explaining the choice of these procedures for realization of the tasks follow,

a) Thresholding - the background level is estimated from the image intensity distribution. At the current stage of the program, this level is manually adjusted for fixed conditions that influence the distribution (e.g. fixed illumination intensity, given optical magnification and given cell line).

b) Median filter – its advantage is that it preserves sharp objects edges during noise reduction.

c) Opening transformation, ancillary to the median filter method. It is used, if required, to separate narrowly connected objects and to remove small objects, which are smaller than cells but bigger than debris removed by the median filter.

d) Perpendicular Sobel operators are used to find the edges of objects.

e) Hough transform used for final precise determination of coordinates of cells.

f) Clustering – a fast-working alternative for Hough transform.

Image recognition should bring exact image coordinates of cells (or cells nuclei), mapped subsequently into real world. For this purpose, the most commonly used method

is currently the Hough transform, since it may be used for detection of presence (and, of course, locations) of virtually arbitrary shapes in the image.

The idea of the the Hough transform is searching local maximums in a special parameter space according to the following algorithm. Since cells have circle-like shape, the space is defined as a three dimensional array *(a, b, r)* of circle origins *(a, b)* and radii *r*. Thus, a circle present in the image corresponds to only one point in the parameter space. If an edge pixel *(x, y)* belongs to a circle, the locus of the parameters of this circle will be a right circular cone (it can be seen from the equation of a circle: $(x-a)^2+(y-b)^2=r^2$ by treating *x* and *y* as fixed and letting *a, b* and *r* vary). Thus, examining every pixel of the image and finding pixel with the color of the objects (white color in our case), we draw the corresponding cone in the parameter space. The more regular is the object contour, the more cones are drawn in the space. Afterwards, the intersection of all cones will correspond to the sought circle parameters.

The great advantage of Hough transform is its quite precise object detection even on the poor quality images [23] (e.g. noise images, images with destructed or partially overlapped objects). On the other hand, the direct realization of this method is very time–consuming and the calculation time grows significantly with the increasing of the object's degree of freedom. Therefore, in spite of the fact that searching for elliptical shapes is more adequate for cells localisation, there are good reasons to apply the Hough transform rather for circle detection.

Moreover, the restriction of circles radii values to a reasonable range (corresponding to typical cell dimensions) reduces the computing power requirements. To further approach a satisfactory performance of the code, several modifications of the Hough transform are realized and tested experimentally, such as direct Hough transform (HT) [24], random Hough transform (RHT) [25], generalized Hough transform (GHT) [26, 30], random circle detection (RCD) [27, 28]. According to the tests performed for cell lines planned to be irradiated in IFJ, the fastest results are achieved by GHT. Unfortunately, even this modification has high time requirement for large image processing (about 35 seconds for 1.3 megapixels image using a Mobile AMD Sempron(tm) 3000+ computer).

As a fast alternative method (only about 5 seconds for 1.3 megapixels image using the same PC), we used clustering (see line C in Fig.7). This algorithm is based on the iteration of standard Erosion method [21, 22] for a circle (r = 1 pixel) as a structuring element until all objects are removed. In this algorithm, all removed neighbouring pixels are collected in one cluster. It means that every pixel on a binarized image is analysed, one by one, on an object colour. When such pixel is found it is removed storing its coordinates in a new cluster; after that we analyse all neighbouring pixels at the same way until all pixels corresponding to the object are removed. As a result, the objects are found in the form of a group of clusters. The clustering has some advantages over the Hough transform: (i) it is about 7 times faster, (ii) the time of calculation is not affected by objects shape. However, the disadvantages are also serious, particularly, it interprets noise as objects and partially overlapped objects as one object. This method requires the post-processing of the image, such as filtering of recognized objects by given size, shape and other parameters.

The time performance comparing clustering and GHT algorithms is shown on Fig.7.

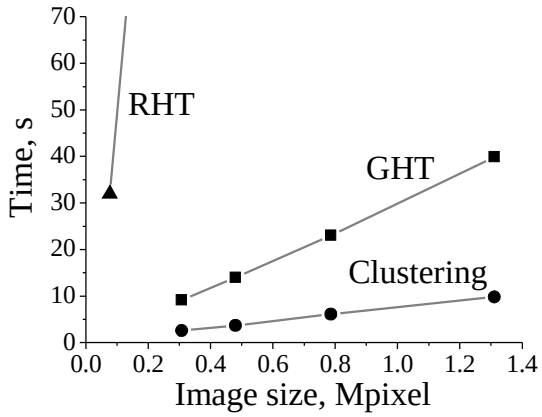

Fig.7 The time performance for cells image processing sequences based on GHT and clustering.

The flexibility of the software allows custom creation of different sequences of presented procedures for image processing. Thus, it achieves the optimal ratio between the time and the effectiveness of calculations. As a final result, the coordinates of the found objects are used for their subsequent irradiations.

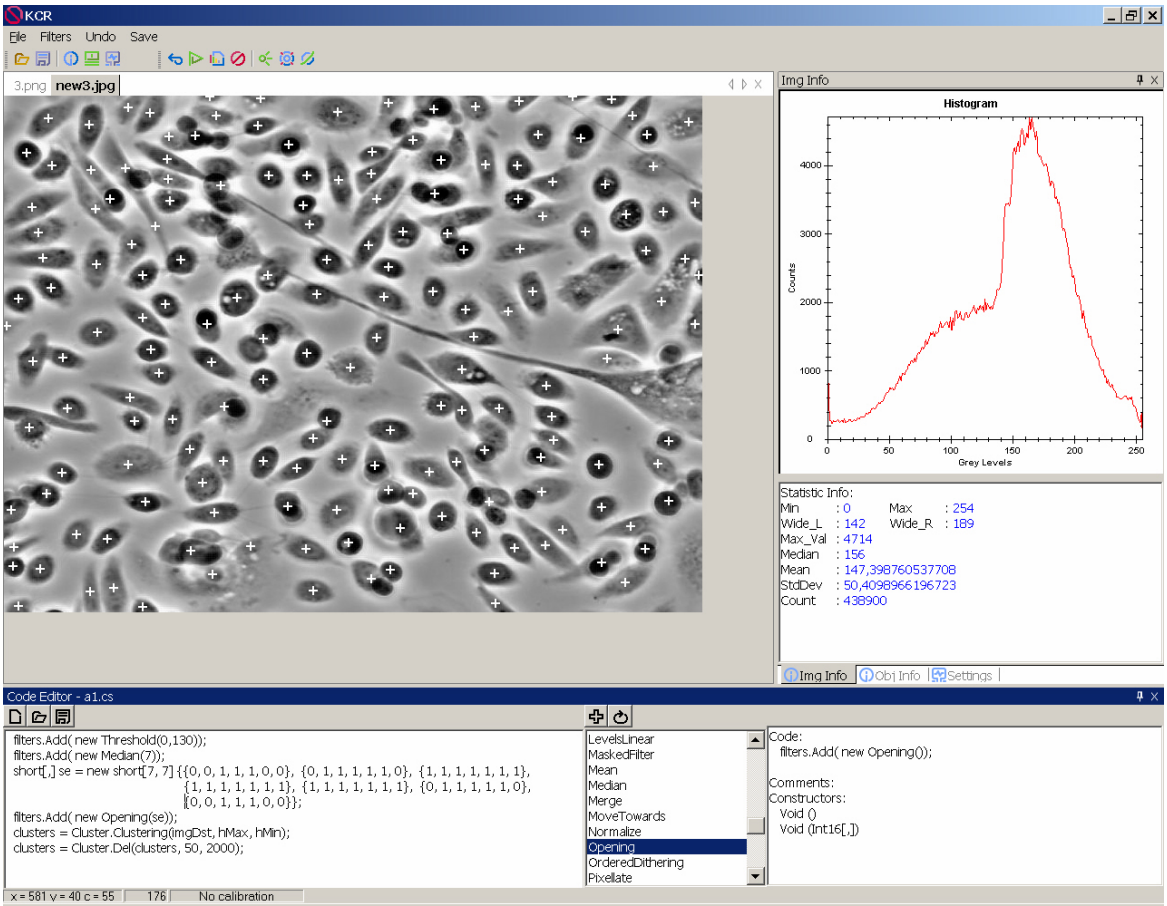

Fig.8. *The screenshot of the Cracow cell recognition program with the processed image of cells (800x600 pixels, 480x385 μm^2). Bottom part of the screenshot demonstrates example of custom command script used for image processing.*

Irradiation process

The irradiation process involves the precise interaction between hardware [17] and software. The first task is to find the position of the beam in the plane of a sample. One of important facts is that although the Zoom125C system provides different magnifications (up to 12.9x), the best positioning precision can be achieved only when using the same magnification for the whole tuning process. The preliminary beam position is obtained after its focusing on a quartz window located off–axis of the experimental chamber (2 cm left to the ions exit window, see Fig. 2). For this task, the experimental chamber is rotated by 5 degrees from its axis. Then the chamber is rotated back to the central position to allow passing the ions through the exit window. However, the use of quartz window defines well the required beam position only if the beam falls strictly perpendicular both to quartz and sample planes. Any imperfections of the relative directions cause the shift of the beam position in the sample plane. Therefore, an additional method for beam localisation was developed. This method is based on automatic scanning of the region of the beam spot on the quartz by a diaphragm (down to a 5 μm diameter) placed in the plane of the sample in such a way that the beam can reach the particle detector located behind the diaphragm only passing through the hole. The diaphragm position where the detector registers the strongest signal corresponds to the centre of beam position. A difference between the beam spot positions (determined optically with the quartz and measured using the scanning method) was found to be up to 60 μm that shows an importance of this adjusting. After removing the particle detector, the diaphragm hole is observed using the optical microscope in transmitted light coming from the photodiode mounted inside the measurement chamber. Since the optical system has a fixed field of view for a fixed magnification, one can store such image of the diaphragm and use it for the subsequent determination of cells position relatively to the beam position.

The previously determined cell coordinates form a map of targets. Just after the recognition process, the map is still in pixel units (not micrometers suitable for positioning table control program). In order to transform these coordinates to micrometers, an important step is the image calibration. For this purpose it is possible to use two methods. The first one is a classical calibration using an optical standard placed in the plane of sample. The second one is more sophisticated. It uses again the diaphragm and utilises the fact that the precision of the positioning stage is about 0.1 μm. The procedure requires taking three photographs of the diaphragm hole. The first photo is used as an origin. The second one, taken after moving the stage along X axis on a certain distance (e.g. 300 μm rightwards), is used for horizontal calibration. The third photo, taken after moving the stage along Y axis (e.g. 200μm downwards), is used for vertical calibration. It is necessary to notice that the choice is the smallest diaphragm for the precise beam position determination and the precise calibration does not give the best results if automatic method based on the Hough transform is used. Better performance was achieved using the 20 μm diameter diaphragm. It can be explained by a fact that the more image pixels correspond to the diaphragm hole, the more precisely the Hough transform can detect this object. In addition, such automatic method is more precise than any manual method. Moreover, the beam current after the 20 μm can be diaphragm several times higher than after the 5 μm diaphragm, consequently the calibration using 20 μm diaphragm requires much less time.

After preparing the map of targets and choosing the required number of ions per single cell, the remaining flowchart of the irradiation process is as follows:

- turn the beam off before the beginning of the experiment with living cells to avoid accidental and unwanted irradiations;

- place the stage in the position of the first target from the map;
- switch the beam on and wait until the counter of pulses coming from the ions registered by the detector achieves the chosen value (in extended part of the program it is possible to select the option when the beam is turned off during incrementing and analysing the counter. This can improve the purity of the experiment). An alternative, but far less accurate method to control the number of ions irradiating thick samples (when ions are not able to reach the detector) uses switching the beam on for a certain period of time which depend on the beam current;
- turn the beam off and place the stage to the next target position;
- repeat steps 3 and 4 for all targets.

The whole irradiation process is controlled by a computer using a specialized software, which allows to make some modifications and additional tools to extend the field of the SIHF applications. One of such additional functions can generate the maps of different patterns. A grid pattern can be used for simulation of broad beam irradiation.

Tests of the system.

Before irradiation of living cells, it is necessary to provide several tests and control experiments to check each part of the system and its overall performance.

To test the blanking system, the following experiment was performed: in a low current mode (10^3–10^4 ions/sec), after registering an ion passage by the particle detector the beam was switched off. However, the system continued registering particles passing to the detector. For statistically significant results such experiment was repeated several times for different beam intensities (see Fig.9).

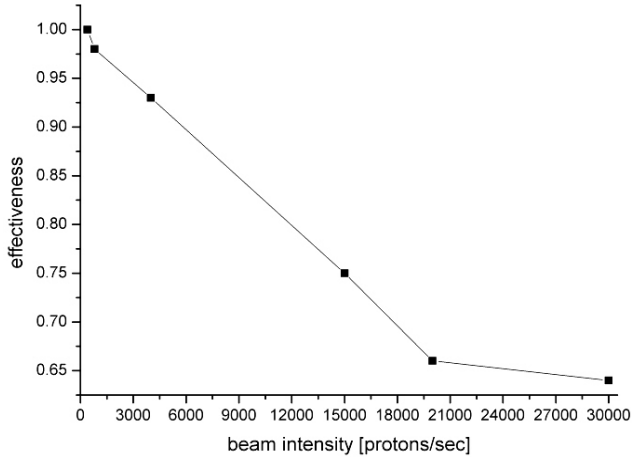

Fig.9 *The effectiveness (the ratio between adjusted number of ions and the obtained number of ions) of the blanking system for different beam intensities.*

The mean value of detected protons per one deflecting event does not exceed 1.02, for intensities of the beam up to 800 protons/sec which is an acceptable performance for our purposes. The measured system reaction time, between the pulse from the detector and the appearance of high voltage (440 V) on deflection plates, is about 23 μs.

In spite of the high precision of the moving stage guaranteed by the manufacturer, the accuracy of the positioning system was tested. First, the diaphragm was set in start position which was determined by the automatic recognition. Then, the stage was positioned in a loop sequence in such a way that after passing trough randomly generated map of targets (thus simulating cells irradiation) it returned to the initial position. After completing the loop, the difference between initial and final positions was measured. As a result, in 99% of cases, independently of the map sizes, stage returned back with

precision not worse than 0.5 μm

Final test was the determination of the beam profile using the diaphragm with 5 μm diameter hole in order to prove the regular (Gaussian) beam intensity shape. This test was carried out in a manner very similar to the beam position localisation described above. An example of the measured beam profile is presented in Fig.10. Such profile can be used to obtain the information about spatial changes in the beam form, the beam direction etc.

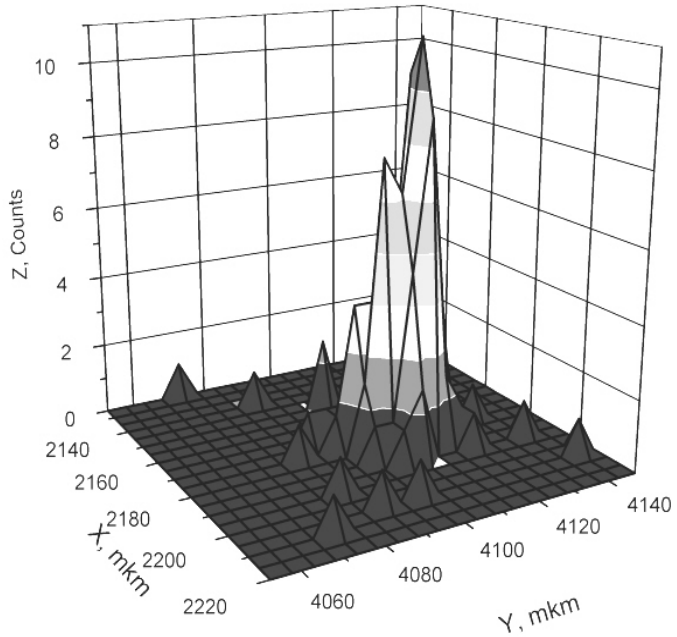

Fig. 10 *An example of beam profile (200 μm from the exit window).*

Results of first irradiations

For the first experiments the human skin fibroblasts (CCL-110) and the well differentiated gastric adenocarcinoma (MKN-7) cells are used. The CCL-110 cells are maintained in DMEM medium supplemented with 10% fetal bovine serum (FBS), L-glutamine and antibiotics. The MKN-7 are grown in RPMI-1640 medium supplemented with 10% FBS and antibiotics. All cells are incubated at 37°C in an atmosphere with 5% CO_2.

For cell irradiation, two types of dishes have been designed and are used. Both designs guarantee that protons reach the detector after traversing a cell. The first type Petri dish has a Si_3N_4 window (500 nm thick) glued over a hole perforated in the centre of a dish bottom. The other design has the bottom made of Mylar foil (2 μm). Two days before an experiment the dishes are sterilized: they are incubated in 70% ethanol for 10 minutes and afterwards exposed to UV for 15 minutes. One day before an experiment the dishes with Mylar film are pre-treated with medium solutions (DMEM or RPMI depending on the type of cells) and then they are kept in the thermostat. The same day cells are treated with a trypsin in order to detach them from the Petri-dish surface and seeded.

Cells are stained with Propidium Iodine and Hochest 33342 fluorescent markers that make possible to distinguish between living and dead cells using fluorescent microscope. The fluorescent pictures of several chosen regions with deposited cells are taken directly before the irradiation. Next, the part of medium is removed from the Petri dish, since the protons cannot pass through a thick layer of liquid. To prevent contamination during irradiation, the Petri dishes are covered with a Mylar foil. Our preliminary tests have shown that such precautionary measure elongates the cells life up to about 30 minutes

under experimental conditions. The first irradiation experiments have been carried out according to the algorithm described previously.

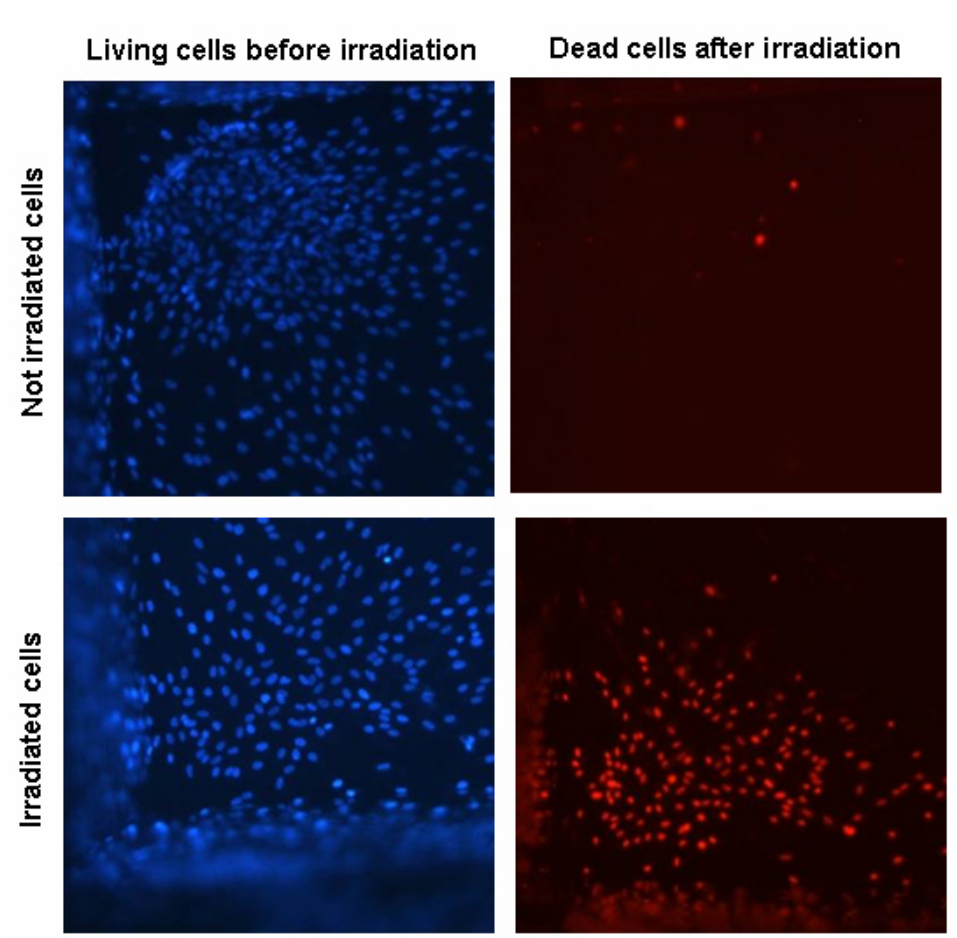

Fig.11 *The examples of irradiated and non-irradiated MKN-7 cells: before and after experiment.*

The number of protons per cell ranged from 50 to 300, what corresponds to a dose of a fraction of a Grey. To exclude the spontaneous cell death, the time of one experiment is kept below 10 minutes and after each experiment the cell dishes, after refilling the medium, are immediately placed back into the incubator. The pictures of irradiated and non-irradiated regions are taken immediately after irradiation, 30 min, and 24 h after irradiation. The analysis of the pictures taken before and after the experiments is carried out using our software. It showed the difference (about 60%) of dead cells percentage in the non-irradiated (control) and irradiated regions 24 hours after experiment (Fig.11).

Conclusions

The described optical and positioning systems provide a firm basis for irradiation of single cells at the Single Ion Hit facility at IFJ PAN. Beam blanking system has a very good performance for ion currents in the range of 1000 ions/sec, suitable for precise irradiation. Beam profile (important factor for ion hit resolution) is regular, but should be improved i.e. beam spot size must be further diminished. Accuracy of the positioning system is sufficient, however special procedures must be applied in order to avoid errors and shifts during calibration from pixel coordinates (given by on-line optical setup) to length units (suitable for positioning system). The software for image processing is very

flexible and easy to use, however the performance of automatic cell recognition system strongly depends on type (shape) of chosen objects and gives best results for regular, circularly shaped cells. Usually, not all cells in a dish may be recognized in a reasonable image processing time, but such requirement is not needed in most of typical irradiation studies. First experiments performed have justified and confirmed the system applicability in single ion irradiations of biological material.

Acknowledgements

This study was supported by the EU 6th Programme grant CELLION, No. MRTN-CT-2003-503923.

References.

[1] M. Folkard, K. Prise, G. Schettino, C. Shao, S. Gilchrist and B. Vojnovic, Nucl, Nucl. Instr. and Meth. in Phys. Res. B **231**, 189 (2005).

[2] J. Soto, C. Sainz , S. Cos and D. G. Lamuno, Nucl. Instr. and Meth. in Phys. Res. B **197**, 310 (2002).

[3] H. Nagasawa and J.B Little, Cancer Research **52**, 6394 (1992).

[4] J. B. Little, Carcinogenesis **21**, 397 (2000).

[5] E.I. Azzam, S.M. de Toledo, A.J. Waker and J.B. Little, Cancer Res. **60**, 2623 (2000).

[6] M. Folkard, G. Schettino, B. Vojnovic, S. Gilchrist, A.G. Michette, S.J. Pfauntsch, K.M. Prise and B.D. Mi-chael, Radiat. Res. **156**, 796 (2001).

[7] H. Zhou, G. Randers-Pehrson, C.A Waldren, D. Vannais, E.J. Hall and T.K. Hei, Proc. Natl. Acad. Sci. USA **97**, 2099 (2000).

[8] L.J. Wu, G. Randers-Pehrson, A. Xu, C.A. Waldren, C.R. Geard, Z. Yu and T.K. Hei, Proc. Natl. Acad. Sci. USA **96**, 4959 (1999).

[9] T.K. Hei, L.J. Wu, S.X. Liu, D. Vannais, C.A. Waldren and G. Randers-Pehrson, Proc. Natl. Acad. Sci. USA **94**, 3765 (1997).

[10] C. Shao, Y. Furusawa, Y. Kobayashi, T. Funayama and S. Wada, The FASEB Journal **17**, 1422 (2003).

[11] M. Folkard, B. Vojnovic, K.M. Prise, A.G. Bowey, R.J. Locke, G. Schettino and B.D. Michael, Int. J. Ra-diat. Biol. **72**, 375 (1997).

[12] M. Folkard, B. Vojnovic, K.J. Hollis, A.G. Bowey, S.J. Watts, G. Schettino, K.M. Prise and B.D. Michael, Int. J. Radiat. Biol. **72**, 387 (1997).

[13] M. Folkard, G. Schettino, B. Vojnovic, S. Gilchrist, A.G. Michette, S.J. Pfauntsch, K.M. Prise and B.D. Michael, Radiat. Res. **156,** 796 (2001).

[14] S.Lebed, Z.Stachura, M.Cholewa, G.J.F.Legge, J.Lekki, S.Maranda, A.Potempa, C.Sarnecki, Z.Szklarz, J.Styczeń and B.Sulkio–Cleff, Nucl. Instr. Meth. In Phys. Res. B **181**, 95 (2001).

[15] J.Lekki, R.Hajduk, S.Lebed, A.Potempa, T.Pieprzyca, Z.Stachura, M.Ziębliński and J.Styczeń, IFJ Report **1856/AP**, (2001).

[16] J.Lekki, M.Cholewa, E.Dutkiewicz, A.Gwiazdowska, R.Hajduk, K.Irzyńska, S.Lebed, P.Mazur, W.Polak, A.Potempa, T.Pieprzyca, C.Sarnecki, Z.Szklarz, A.Veselov, R.Zając, Z.Stachura and J.Styczeń, IFJ Report **1915**, (2002).

[17] W. Polak, R. Hajduk, S. Lebed, J. Lekki, T. Horwacik, S. Maranda, T. Pieprzyca, C. Sarnecki, Z. Stachura, Z. Szklarz, O. Veselov and J.Styczeń, IFJ Report **1955/AP**, (2004).

[18] O. Veselov, J. Lekki , W. Polak , D. Strivay , Z. Stachura , K. Lebed and J. Styczeń, Nucl. Instr. and Meth. in Phys. Res. B **231**, 212 (2005).

[19] http://www.dipol.com.pl/esklep/m10765.htm

[20] E.D. Barone-Nugent, A. Barty, K.A. Nugent, J. Microscopy **206**, 194 (2002).

[21] C.Gonzalez, E.Woods, Digital Image Processing, 2nd ed. (Prentice Hall, New Jersey,2002).

[22] William K. Pratt. Digital image processing. (A Wiley-Interscience publication John Wiley and Sons, New York, 1978).

[23] D. Walsh and A.E. Raftery, Pattern Recognition **35**, 1421 (2002).

[24] P.V.C. Hough, US Patent **3069654**, (1962).

[25] R.A. McLaughlin,Pattern Recognition Lett. **19**, 299 (1998).

[26] D. H. Ballard, Pattern Recog. **13**, 111 (1981).

[27] Teh-Chuan Chen and Kuo-Liang Chung, Computer Vision and Image

Understanding **83**, 172 (2001).

[28] S.-C. Zhang and Z.-Q. Liu, Pattern Recognition **38**, 273 (2005).

[29] R.O. Duda and P.E. Hart, Commun. ACM **15**, 11 (1972).

[30] P.R. Barber, B. Vojnovic, J. Kelly, C.R. Mayes, P. Boulton, M. Woodcock, and M.C. Joiner, Phys Med Biol **46**, 63 (2001).

[31] T. Reinert, A. Fiedler , J. Skopek , J. Tanner , J. Vogt and T. Butz, Nucl. Instr. and Meth. in Phys. Res. B **219–220**, 77 (2004).

[32] K.-D. Greif, H. J. Brede, D. Frankenberg and U. Giesen, Nucl. Instr. and Meth. in Phys. Res. B **217,** 505 (2004).